Invited paper for the Symposium on the Macroscopic Features of Heavy Ion Collisions and the Pre-equilibrium Process, Hakone, Japan, September 1977.

CHARGE AND ANGULAR DISTRIBUTIONS AS WELL AS SEQUENTIAL DECAY AND γ-RAY EMISSION IN HEAVY ION COLLISIONS VIEWED IN THE LIGHT OF THE DIFFUSION MODEL

L. G. Moretto†

The Department of Chemistry
and
Lawrence Berkeley Laboratory
Berkeley, California 94720

ABSTRACT

The hierarchy of the collective relaxation times in heavy ion reactions is briefly reviewed. An improved diffusion model is introduced and applied to interpret the fragment Z and angular distributions for some typical reactions. The equilibrium in the neutron-to-proton ratio as well as the sharing of the excitation energy between fragments is studied by a coincidence method which leads to the measurement of the charge, mass and mean number of nucleons emitted by each fragment. The final destiny of the dissipated energy is determined by measuring the atomic number of two coincident fragments, thus obtaining the missing charge as a function of bombarding energy and the Q of the reaction. The sequential fission probability of the heavy recoil is established as a function of the Z and kinetic energy of the light partner. The out-of-plane angular distribution of the fission fragments is correlated with the fissionability and interpreted in terms of various sources of angular momentum misalignment.

The γ-ray multiplicities and γ-ray angular distributions associated with deep inelastic event are discussed in terms of the angular momentum transfer and in terms of the diffusion model.

† Sloan Fellow 1974-76, extended support.

INTRODUCTION

The great variety of relaxation processes associated with collective modes discernable in heavy ion reactions has made this field perhaps the liveliest in the realm of nuclear physics.[1,2] A hierarchy of relaxation times has been more or less established for the various degrees of freedom of the intermediate complex. The relaxation of the neutron-to-proton ratio and of the relative motion appear to be fastest, followed by the rotational degrees of freedom and trailed by the mass asymmetry degree of freedom. This last mode has been investigated in a large number of one-fragment inclusive reactions. Usually the Z of one of the fragments is identified and its angular distribution provides information of the time scale of its production. It appears that the time evolution of this mode is diffusive in its nature and describable in terms of a transport equation, like the Master equation or the Fokker-Planck equation.[1,3,4]

In the first part of this paper a diffusion model, designed to reproduce the Z and angular distributions will be presented and its predictions shall be compared with some of our experimental data.[5]

Coincidence experiments have provided us with the possibility of studying the degree of relaxation of the E1 mode associated with the neutron-to-proton ratio of the two fragments through the simultaneous measurement of the fragment mass and charge. Also the problem of thermal equilibrium between fragments can be investigated by such experiments as well as the ultimate fate of the excitation energy.[6]

As an example, in part two of this paper some coincidence studies on the reaction ^{Nat}Ag + 340 Mev ^{40}Ar will be illustrated.[6] It will be concluded that, in the explored angular range, the two fragments have

the same temperature and their neutron-to-proton ratio is at equilibrium.

In part, three, the study of the reaction $^{Nat}Ag + ^{20}Ne$ at 158, 252, 343 Mev by means of the simultaneous identification of the atomic number of both fragments will illustrate the final fate of the excitation energy.

Somewhat related to the experiments described in part two and three is the study of sequential fission presented in part four. The fissionability of the heavy recoil in the reaction ^{197}Au + 620 Mev ^{86}Kr is measured for each Z of the light partner as a function of the light partner kinetic energy[8]. From the dependence of the fissionability upon atomic number and energy, information is obtained regarding the excitation energy and the angular momentum of the fissioning nucleus and thus on energy and angular momentum transfer. Interesting light on the exit channel oscillations of the intermediate complex and on the fragment depolarization is shed by the out-of-plane fission fragment angular distributions.

A more detailed information on the equilibration of the rotational modes is obtained through the measurement of the γ-ray multiplicity as a function of Z and energy.[9,10] Examples of these experiments are presented in part five. In this part the problem of angular momentum alignment of the fragments will also be discussed, as well as the use of the Z dependence of the γ-ray multiplicity as a tool to test the diffusion mechanism along the mass asymmetry degree of freedom.

This presentation is meant to be a brief overview of the heavy ion studies being conducted in our group at Berkeley.

I. THE CHARGE AND ANGULAR DISTRIBUTIONS

The Diffusion Equations

We assume that the intermediate complex has a shape close to that of two touching fragments.[1,3] Charge to mass equilibration is assumed. We further assume that the time evolution along the asymmetry coordinate is diffusive in nature and describable in terms of the Master Equation:

$$\dot{\phi}(Z,t) = \int dZ' [\Lambda(Z,Z')\phi(Z') - \Lambda(Z',Z)\phi(Z)] \quad , \tag{1}$$

where $\phi(Z,t)$, $\dot{\phi}(Z,t)$ are the populations of the configurations characterized by the atomic number Z of one of the fragments, and their time derivative at time t; and $\Lambda(Z,Z')$, $\Lambda(Z',Z)$ are the macroscopic transition probabilities.

If in eq. (1) one writes: $Z' = Z + h$ and all the quantities are expanded about Z in powers of h, one obtains to lower order:

$$\dot{\phi}(Z,t) = \frac{\partial}{\partial Z}\left[\mu_1 \phi\right] + \frac{1}{2}\frac{\partial^2}{\partial Z^2}\left[\mu_2 \phi\right] \tag{2}$$

which is the well-known Fokker-Planck equation. The quantities μ_1 and μ_2 are the first and second moments of the transition probabilities:

$$\mu_1 = \int h\Lambda(Z,h)dh \quad ; \quad \mu_2 = \int h^2\Lambda(Z,h)dh \tag{3}$$

An analytical solution is available when the force is harmonic or:

$$V_Z = \frac{c}{2}(Z-Z_{sym})^2 = \frac{1}{2}ch^2 \quad ; \qquad (4)$$

the solution is:

$$\phi(h,t) = c^{1/2}\left[2\pi T\left(1-\exp-\frac{2ct}{K}\right)\right]^{-\frac{1}{2}} \exp - \frac{c[h-h_o \exp -ct/K]^2}{2T(1-\exp-2ct/K)} \qquad (5)$$

Where T is the temperature and K is the friction coefficient. Also we have made use of the Einstein relation $\mu_1/\mu_2 = -V_Z'/2T$ where $-V_Z'$ is the force along the mass asymmetry coordinate.

The transition probabilities

From general phase space considerations one can consider the following ansatz for the transition probabilities[1]:

$$A(Z,h) = \kappa f \exp - V_Z'h/2T \qquad (6)$$

The Fokker-Planck coefficients can then be calculated:

$$\mu_1 = -2\kappa f \sinh V_Z'/2T = -\kappa f V_Z'/T \; ; \; \mu_2 = 2\kappa f \cosh V_Z'/2T = 2\kappa f \qquad (7)$$

which for large T satisfy the Einstein relation.

Such an ansatz implies for the friction coefficient: $K = \frac{T}{\kappa f}$.

Alternatively if the particle transfer between two fragments with chemical potential differing by an energy $a = V'h$ is considered, one can write:

$$\Lambda(Z,h) = Ag \int \frac{d\varepsilon}{1 + \exp(\varepsilon - a)/T} \left(1 - \frac{1}{1 + \exp \varepsilon/T}\right) = \frac{AgV'_Z h}{1 - \exp -V'_Z h/T} \qquad (8)$$

where A is some strength constant and g the average single particle level density. The final result is:

$$\mu_1 = - Ag\, V'_Z \;;\; \mu_2 = Ag\, V'_Z \coth V'_Z/2T \simeq 2\, AgT \qquad (9)$$

again satisfying the Einstein relation. The friction coefficient is:

$K = \frac{1}{Ag\xi}$.

The diffusion constant

If one takes the idea of particle transfer seriously, it is possible to write the particle transfer rate as suggested by Randrup[11]:

$$\kappa f = \int n\, d\sigma = 2\pi\, n_o \bar{R}\, b\, \psi(\zeta) \qquad (10)$$

where n_o is the particle flux in nuclear matter at saturation density, $\bar{R} = \frac{C_1 C_2}{C_1 + C_2}$ is a reduced radius expressed in terms of the central radii of the two fragments, b is the skin thickness and $\psi(\zeta)$ is a universal function depending upon the separation between the sharp surface of the two fragments in units of the surface thickness. This approach neatly factors out the geometrical features of the problem.

The asymmetry potential energy

In general, the potential energy of the intermediate complex as a function of Z can be written as

$$V(Z,\ell) = V_{LD}(Z) + V_{LD}(Z_T - Z) + V_{Prox}(Z,\ell) + V_{Coul} + V_{Rot} \qquad (11)$$

where ℓ is the total angular momentum, V_{LD} represent the liquid drop energies of the two fragments, and V_{Prox} is the nuclear interaction or proximity energy [12].

The total potential V depends on the fissionability of the system x, on ℓ and on the distance between centers D.

The driving force which arises from this potential depends dramatically on the entrance channel asymmetry, as well as on x, ℓ, D. It may either drive the system towards symmetry or towards extreme asymmetries. For a reaction like 600 MeV Kr + Au the driving force is in the direction of symmetry most of the time.

The radial and tangential motion

Both the diffusion constant and the asymmetry potential energy depend upon the distance between the two fragments. This distance is controlled by the radial motion of the system. Furthermore the extent to which the diffusion proceeds depends upon the interaction time. We shall therefore limit ourselves to an extremely simplistic treatment which, however, respects the experimental evidence closely.

The radial potential can be written as:

$$V(D) = V_{Prox} + \frac{Z(Z_T - Z)e^2}{D} + \frac{\hbar^2 \ell^2}{2\mathcal{J}(\ell)} \qquad (12)$$

$\mathcal{J}(\ell)$ being an appropriate moment of inertia.

It is not very clear how much the fragments must interpenetrate before the above equation breaks down. This makes it difficult to formulate the dynamical problem. For the present we shall just use the above potential to calculate the average force $F_R(\ell)$ at the interation distance D_{int}: $F_R(\ell) = \partial V(D)/\partial D\Big|_{D_{int}}$. From the knowledge, at the interaction radius, of the reduced mass μ, of the radial velocity V_R and of the radial force F_R for each ℓ value, one can introduce the following two ansatz for the interaction time τ and the average penetration $\bar{x}$:[5]

$$\tau(\ell) = \frac{2\mu v_R}{F_R} = \frac{2\sqrt{2\mu(E-B)}}{F_R}\left(1 - \frac{\ell^2}{\ell_{max}^2}\right)^{\frac{1}{2}} \; ; \; \bar{x}(\ell) = \frac{\alpha}{2}\frac{\mu v_R^2}{F_R} \qquad (13)$$

When better dynamical calculations become available, it will be a trivial matter to substitute the ansatz in eq. 13 with more reliable expressions.

The diffusion along the asymmetry coordinate is then allowed to proceed with a form factor dependent upon $\bar{x}(\ell)$ for a time $\tau(\ell)$.

The tangential motion is treated assuming for the equation of motion the simple form:[5]

$$F_T = \mu\gamma(\omega_o - \omega_{Rig}) \tag{14}$$

where ω_o and ω_{Rig} are the two limiting orbital angular velocities corresponding to sliding and sticking.

The constant γ is chosen such as to approximately reproduce the mean kinetic energies as a function of angle assuming that all of the radial energy is lost.

Results of the calculations

The interaction times calculated for the reaction Au + Kr at three energies are shown in fig. 1a as a function of angular momentum. There is good experimental evidence for the angular momentum dependence predicted by our ansatz. It is interesting to notice the rather mild average increase in lifetime with increasing bombarding energy. In Fig. 1b the average deflection function is shown. Notice the well pronounced deep inelastic rainbow which moves from positive to negative angles as the bombarding energy increases. The 600 MeV curve, predicting a rainbow angle of about 50° is in excellent agreement with experiment. The

movement of the rainbow angle towards smaller and eventually negative angles results from the combination of three factors: i) creasing lifetime; ii) increasing angular momentum; iii) decreasing average moment of inertia due to the increasing average penetration. In figs. 2a,b the calculated angle-integrated Z distributions are compared with experiment for the reactions Au + Kr^{13} and Ta + Kr^{14} at 620 MeV. The agreement is reasonable over more than two orders of magnitude. Some of the apparent discrepancies arise from the fact that the experimental angular distributions have been integrated over an incomplete angular range. In figs. 3a and b, examples of the angular distributions for fragments of various Z are shown for both reactions. The theory nicely tracks the experiment in predicting forward peaked angular distributions at small Z's which develop into side-peaked angular distributions close to the projectile. For Z's above the projectile, the angular distributions slowly lose their side peak and return forward peaked. The satisfactory reproduction of both the Z distributions and the angular distributions shows that the calculated dependence of the interaction times and of the diffusion constant upon angular momentum and radial velocity is reasonably good.

II. MASSES, CHARGES AND PARTITION OF EXCITATION ENERGY BETWEEN FRAGMENTS.

We have already discussed the fact that the fragment charge-to-mass ratio, being essentially a El collective mode, should have high frequency and should quickly equilibrate. We have also commented on the fact that the kinetic energy associated with the relative motion is rapidly dissipated. It is interesting to determine whether the Z/A ratio of the emitted fragments does indeed correspond to a relative minimum in the potential energy at fixed mass asymmetry and whether the excitation energy of the fragments corresponds to thermal equilibrium or isothermicity.

After the break-up of the intermediate complex, the fragments are highly excited and are expected to emit neutrons, protons, and α particles through the evaporation process. A detailed investigation of the charges and masses of the fragments as well as their charge and mass loss through evaporation allows us to learn about the fragment neutron-to-proton ratio and the sharing of the excitation energy between the two fragments. A coincidence experiment was performed on the system $^{40}Ar + {}^{Nat}Ag$ at 340 Mev bombarding energy in which the measurement of the Z of the light fragment, along with the energies and angles of both fragments permits the determination of the masses before evaporation and some insight in the evaporation process.[6]

The ^{40}Ar beam of the SuperHILAC with an energy of 340 MeV was used to bombard a natural, self-supporting, 350 $\mu g/cm^2$ Ag target. Two detectors measured the light and heavy fragment energies and angles in coincidence. The light fragment detector, which consisted of an ionization chamber telescope, measuring both energy (E_3) and the atomic number (Z_3), was placed at 42° from the beam direction.

On the other side of the beam axis, a high resistivity silicon position sensitive detector (PSD) was placed parallel to the reaction plane and successively at 30° and 50° from the beam axis to explore the 20° - 60° in plane distribution of the correlated heavy fragment. The measured quantities were the energy (E_4) and the in-plane angle (θ_4) of the heavy fragment.

Out-of-plane angular distributions were also measured keeping the light fragment telescope at the same angle (42°), but at three different angle settings of the position sensitive detector (29°, 42° and 50°).

Very accurate energy measurements are necessary in this experiment. While the pulse height defect (PHD) is very small for low Z ions detected in silicon, it is significantly higher for a high Z ion of the same kinetic energy. In a calibration experiment, a beam of 163 MeV Ar from the 88" LBL cyclotron was incident on thin (200 to 350 $\mu g/cm^2$) self supporting foils of natural gold, silver, and copper. The observed energies of the elastically scattered nuclei, were corrected for energy defect due to dead layers and target and window thicknesses and were then compared to the calculated elastic energies of both nuclei and the differences were attributed to the PHD.

A critical test of the accuracy of the energy corrections for heavy ions is the ability to reproduce the kinematics of elastic scattering. The results of correlated elastic scattering measurements made with 163 MeV Argon incident on gold, silver and copper targets are shown in fig.(4). The agreement with calculations (solid lines) is good except when the recoil energy drops below about 15 MeV.

In the case of a binary breakup of the intermediate complex, the conservation of linear momentum and mass can be expressed through the following set of equations in the LAB system:

$$E_3^* A_3^* = A_1 E_1 \frac{\sin^2 \theta_4}{\sin^2(\theta_3 + \theta_4)} \tag{15}$$

$$E_4^* A_4^* = A_1 E_1 \frac{\sin^2 \theta_3}{\sin^2(\theta_3 + \theta_4)} \tag{16}$$

$$A_3^* + A_4^* = A_1 + A_2 \tag{17}$$

The energy E_i of a primary fragment of mass A_i^* becomes on th average after evaporation of $\bar{\nu}_i^T$ nucleons of mean energy $\bar{\eta}_i$

$$\bar{E}_i = E_i^* \left(1 - \frac{\bar{\nu}_i^T}{A_i^*} \left(1 - \frac{\bar{\eta}_i}{E_i^*}\right)\right) \tag{18}$$

The second term of the inner brackets represents the recoil corrections which are small (6%) in our experiment. To first order equation (18) can be written as: $E_i^* = \bar{E}_i \left(1 + \frac{\bar{\nu}_i^T}{A_i}\right)$.

If we define:

$$K_i = \frac{E_1 A_1}{\bar{E}_i} \frac{\sin^2 \theta_j}{\sin^2(\theta_i + \theta_j)} \qquad \begin{matrix} i = 3,4 \\ j = 4,3 \end{matrix} \tag{19}$$

which contains all measured quantities, Eq. (14) to (17) become:

$$A_3^* + \bar{\nu}_3^T = K_3 \tag{15}$$

$$A_4^* + \bar{\nu}_4^T = K_4 \tag{16}$$

$$A_3^* + A_4^* = A_1 + A_2 \tag{17}$$

This set of equations shows that the total number of evaporated nucleons from the two fragments ($\bar{\nu}_3^T + \bar{\nu}_4^T$) can be obtained to first order without any assumptions on A_3^* and A_4^*. This simple analysis yields the values plotted in Fig. 5 as a function of the Z of the light fragment. The quantity $\bar{\nu}_3^T + \bar{\nu}_4^T$ appears to be reasonably constant throughout the Z range of this experiment.

Since atomic numbers have been resolved up to Z = 32, data are available for nearly symmetric break-up. Near symmetry it is reasonable to assume that the relative loss of mass $\frac{\bar{\nu}^T}{A^*}$ is the same for both fragments. With this assumption and Eq. (15) to (18), the masses of both fragments $A_{3,4}^*$ prior to particle evaporation, and the total number of evaporated nucleons $\bar{\nu}_{3,4}^T$ can be calculated for each fragment using the experimental data. The results of these calculations are shown in fig. 6. It is interesting to notice that a sizable discontinuity is visible in the masses at symmetry. This is an indication of the evaporation of charged particles. Since the fragments should be identical at symmetry, the number of evaporated charges per fragment is given by the downward and upward shift in Z that must be applied to the two branches so that they coincide. This shift is 1.3 charge units per

fragment. In Fig. 6 such a shift has been applied, thus generating a continuous curve. Evaporation calculations predict an average of 1.2 evaporated charges at symmetry in good agreement with our data.

In order to extract the masses and number of emitted particles from the data away from symmetry, the assumption made in the previous paragraph, namely that the ratio $\frac{\nu^T}{A^*}$ is the same for the two fragments, is not necessarily valid. Instead we can use the conservation of the energy in the laboratory system, assuming again a binary splitting of the system. The conservation of energy can be expressed as:

$$E_1 + B(A_1, Z_1) + B(A_2, Z_2) = E_3^* + E_4^* + B(A_3^*, Z_3^*) + B(A_4^*, Z_4^*) + E_n^T + E_p^T + E_\alpha^T + E_\gamma^T \quad (20)$$

where: E_3^* and E_4^* can be calculated from Eq. (18); $B(A^*, Z^*)$ is the binding energy of a fragment of mass A^* and charge Z^* before evaporation. E_n^T, E_p^T, E_α^T, E_γ^T are the total excitation energies released by the fragments in the evaporation of neutrons, protons, alpha particles and γ-rays, respectively.

Using Eq. (20), along with Eqs. (15) to (18) in which now one must read:

$$\nu_{3,4}^T = \bar{\nu}_{3,4}^n + \bar{\nu}_{3,4}^p + 4\,\bar{\nu}_{3,4}^\alpha \ ,$$

a self-consistent procedure was developed to obtain the mass and the number of evaporated neutrons for each fragment.

The results of these calculations are given in fig. 7 which shows the masses prior to evaporation and the number of evaporated neutrons as a function of the Z before evaporation of the fragment. Around symmetry, the agreement with the simple analysis done before (Fig. 6) is good. The upper solid line represents the masses calculated by assuming charge equilibrium between two liquid drops in contact with fixed mass asymmetry. The good agreement with this model confirms that charge equilibrium is indeed achieved in deep inelastic collisions for the part of the angular distribution beyond the grazing angle. The lower solid line represents the calculated value of $\bar{\nu}^n$ from an evaporation code. The good agreement with the experimental values also suggests that thermal equilibrium is achieved between the fragments as was postulated when establishing the input parameters of the evaporation calculations.

Emission of particles before or after the breakup of the system perturbs the direction of the velocity of the fragments and lead to a spreading of the heavy fragment direction in the plane as well as out of the plane of the reaction. The widths of the in-plane and out of plane angular distributions are given by the following expression, in which $\bar{\nu}$ is the average multiplicity, $\bar{\eta}$ the average kinetic energy of the neutrons and E^* is the KE of the fragment of mass number A:

$$\sigma_\theta^2 = \frac{1}{2} \frac{\overline{\nu\eta}}{A^* E^*} \qquad (21)$$

The following first order expression contains contributions from both fragments:

$$\sigma_\theta^2 = \frac{1}{2} \frac{\bar{\eta}_3 \bar{\nu}_3 + \bar{\eta}_4 \bar{\nu}_4}{A_4^* E_4^*} \tag{22}$$

This equation reduces to

$$\sigma_\theta^2 = T \frac{\bar{\nu}_3 + \bar{\nu}_4}{A_4^* E_4^*} \tag{23}$$

if we assume that the nuclear temperatures of the fragments are the same. These calculations are compared to the experimental values in fig. 8.

III. CHARGED PARTICLE EVAPORATION IN DEEP INELASTIC EVENTS THROUGH Z1-Z2 COINCIDENCE STUDIES.

While it was evident from the earliest studies that heavy ion reactions were characterized by large degrees of inelasticity, the final destiny of the missing energy has not been satisfactorily investigated as yet. Most of the experiments performed to date have been focused on the relaxation of collective modes, the mass-asymmetry mode being the most studied. The reason for this state of affairs stems largely from the fact that most of the studies of deep-inelastic collisions (DIC) have been one fragment inclusive experiments in which only the mass or charge of a single fragment has been measured. While it is obvious from the energy spectra of these fragments that much of the entrance channel kinetic energy has been dissipated, it is by no means obvious how this has been accomplished. Recent experiments with ^{14}N and ^{16}O projectiles have hinted that fragmentation processes may be occurring. In order to shed light on the energy dissipation mechanism, we have undertaken a series of coincidence experiments in which both of the primary charged fragments have been identified in Z.[7] The system studied, $^{20}Ne + {}^{63}Cu$, was chosen for a variety of reasons: the charge and angular distributions for singles events have already been measured; it is possible to vary the bombarding energy over a broad range; and the technique of simultaneous Z-determination is optimized for relatively light systems.

A self-supporting 560 $\mu g/cm^2$ thick ^{63}Cu foil (99% enrichment) was bombarded with ^{20}Ne ions produced by the Berkeley 88" Cyclotron. The detection apparatus consisted of two large solid angle (5° angular acceptance) particle telescopes, each having a gas ionization ΔE

detector and a solid state E detector. The gas counters were operated with pure methane at a pressure of 4 cm Hg. The entrance windows consisted of thin (60 $\mu g/cm^2$) polypropylene foils mounted on circular collimators 1 cm in diameter. The initial measurements made with 252 MeV ^{20}Ne ions were aimed at studying the de-excitation products of the symmetric decay mode (i.e. $Z_1 = 19$, $Z_2 = 20$) at near-symmetric angles ($\theta_1 = 42°$, $\theta_2 = 44°$). In this configuration adequate Z-resolution was obtained up to the low 20's.

In addition to the symmetric angle measurements, data were taken over the range of the angular correlation (θ_1 fixed at 42°), both in-plane and out-of-plane. The in-plane correlation is broad (≈15° FWHM). The out-of plane distribution is somewhat narrower, the FWHM being slightly less than 10°. Neither of the quantities varies much as a function of the detected charges. For the 158 and 343 MeV lab energies, measurements were taken only at symmetric angles.

In fig. 9 the Z_2 distribution for fixed Z_1 is plotted for various cuts in the total lab kinetic energy, E_T. The total energy was chosen since it is most closely related to the excitation energy. The FWHM of the distributions is large (≈4-5 charge units), and is approximately constant for different Z_1 and different E_T. The centroids of the distributions exhibit an interesting trend: as E_T is decreased, the position of the centroid moves towards lower Z_2. Presumably, this just reflects the fact that the excitation energy increases for lower values of E_T.

To investigate the in-plane angular dependence as well as the energy dependence of the evaporated charge, the average missing charge ΔZ

(i.e. $39-Z_1-Z_2$) is plotted vs. E_T for various Z_1 and θ_2 (see fig. 10). Several points are immediately obvious: 1) the number of evaporated charges is large, ΔZ ranging from 8-4 as E_T ranges from 60-150 MeV; 2) ΔZ decrease with increasing E_T; 3) the magnitude and shape of the ΔZ curve is essentially independent of the asymmetry of the fragments shown by the clustering of the values for different asymmetries); 4) the above trends do not change appreciably over the in-plane correlation. Point 1) is understandable since we are dealing with a light system (low Coulomb barrier) at high excitation energies. The gross dependence of ΔZ on E_T can be attributed to an excitation energy effect: as the lab energy increases, the available excitation energy decreases so that fewer particles are emitted. The insensitivity of ΔZ on asymmetry is explained by virtue of the fact that the Q values leading to different exit channels for this system are small and essentially independent of asymmetry (assuming constant Z/A for the fragments). The fourth point (i.e. the lack of angular dependence) is probably just an artifact of the evaporation process itself. There is so much evaporation that the width of the in-plane distribution is largely a result of it.

The out-of-plane data (see fig.11) does, however, show angular effects. The symmetric angle setting ($\theta_o = 42$, $\theta_2 = 44°$) is again shown for comparison. For $\theta_2 = 44°$, $\phi_2 = 10°$ the mean evaporated charge ΔZ is slightly higher by about .5 charge units. For $\phi_2 = 20°$ ΔZ has increased by almost 1 Z-unit. (From now on we shall present only the average ΔZ; the "error bars" represent one standard deviation in the spread of the data for the various asymmetries.) It is reasonable to assume that in looking out-of-plane, one is preferentially selecting those events in which more

extensive evaporation has occurred, perhaps via α emission, which tends to impart high recoil momentum. The correlation data can also be used to estimate the total evaporated mass. Simple calculations yield 15 ± 3 units of evaporated mass. The large error is due to uncertainties in the angles associated with the large angular acceptance. This result is consistent with preliminary data on light charged particles (p's,d's,α's) which were detected in a third telescope (28 μm ΔE, 5 mm E).

In fig. 12 the average ΔZ is plotted vs. E_T for the three bombarding energies. Again the angles have been chosen at the peak of the correlation for symmetric division. The gross trend favoring higher ΔZ for bombarding energy is, perhaps, to be expected for the resulting higher excitation energies.

It is more important to note that the average ΔZ increases monotonically with bombarding energy. This observation is strong evidence that the incident energy is thermalized over a broad range of bombarding energies. While such behaviour is, perhaps, not unexpected at low energies, it is not obvious that this should be the case at high energies. Another immediate consequence of this data is that DIC are essentially binary over a very broad energy range.

Yet another interesting feature is manifest in this data: the pronounced dip in the 158 MeV curve and the change of slope at intermediate E_T for 252 and 343 MeV data. We believe that this effect is due to the competition between p, α and n emission. For low temperature the difference in the effective barriers between the various decay modes can enhance a particular decay. Since the effective ΔZ/ΔE is different for the various channels (e.g. ΔZ ≈ 0 for n decay), the slope of the

curve can change with E_{γ}. For high temperatures the ratio of the decay widths tends to 1, which accounts for the general observation that minima are not present at higher energies (fig. 13).

IV. SEQUENTIAL FISSION IN DEEP INELASTIC REACTIONS

A recent study of the system 979 MeV ^{136}Xe + ^{197}Au [15] produced evidence of substantial secondary fission of the target-like fragments formed in deep inelastic collisions. These secondary fission events were characterized by an atomic number Z of approximately one half that of the target, a maximum cross section at an angle where the deep inelastic target-like products would peak and a substantially larger than Coulomb energy for angles near this maximum. These observations are consistent with a binary reaction process wherein the initial kinetic energy of the projectile is dampened into internal degrees of freedom. A rotating intermediate complex is formed and nucleons are exchanged between the two excited fragments. The intermediate complex undergoes decay and the two fragments separate. At a later time when the excited heavy fragment has left the nuclear field of the light fragment, it may undergo fission. To investigate whether secondary fission of the Au-like products occurs with a lighter projectile at a lower bombarding energy and to explore in more detail the dependence of the fissionability on the atomic number and the excitation energy of the heavy fragment, we performed a coincidence study of deep inelastic products from the reaction 620 MeV ^{86}Kr + ^{197}Au. [8]

A self-supporting target of ^{197}Au was bombarded with a 620 MeV ^{86}Kr beam from the SuperHILAC and the light and heavy reaction products were detected in coincidence on opposite sides of the beam. A ΔE-E telescope with a 1 msr solid angle was used to measure the atomic number Z_3, the lab angle θ_3 and the energy E_3 of the fragment. The complementary heavy fragment or one of its secondary fission fragments was detected in

coincidence with a large solid angle (~100 msr) X-Y position-sensitive detector which measured the in-plane lab angle θ_4, the out-of-plane angle ϕ_4 and the energy E_4 of this fragment. For binary events the ΔE-E detector localizes the light fragment to $\pm 1°$. Since subsequent neutron evaporation causes only small perturbations, the massive heavy fragment's direction is restricted to a narrow angular region. As a result of this localization of the heavy fragment and of the large solid angle of the X-Y detector, events from a binary reaction process not followed by secondary fission could be detected with an efficiency of essentially 100%. (This 100% detection efficiency was verified with elastic scattering data.) Thus, by comparing the singles to non-fission coincident events for a light fragment of a particular Z, the fissionability of the complementary heavy element can be measured.

In fig.14 some results are shown for a light fragment Z_3 - 38 detected at $\theta_3 = 50°$. The X-Y detector was positioned at -50° and subtended 20° both in and out-of-plane. The entire histogram represents the singles data, the unshaded part represents the non-fission coincidence data and the difference represents the fission component (shaded area). From this figure it is apparent that the probability with which a $Z_4 = 77$ nucleus undergoes secondary fission depends strongly on the energy of the light fragment E_3. For large light fragment energies, very little secondary fission is observed whereas at low energies almost all the heavy fragments undergo secondary fission. Since the excitation energy of the heavy fragment inversely correlates with the light fragment energy E_3, this data indicates that the probability of secondary fission increases

dramatically with the excitation energy of the heavy fragment. In fig. 15 this point is better illustrated. Decreasing the E_3 energy by 140 MeV causes the probability that the $Z_4 = 77$ fragment will undergo secondary fission to increase 0% to 93%.

The extremely high values of the fission probabilities seem to require a sizable depression of the fission barrier due to angular momentum. In other words, fission occurs mainly for the heavy recoil's which have the largest angular momentum, and does not sample the angular momentum distribution uniformly. This is important for the interpretation of the fission fragment angular distributions.

Since the fission barriers for elements above and below Au show a strong Z-dependence, it is interesting to determine the mean fissionability as a function of the number of charge units transferred to or from the target. By integrating over E_3 for each Z_3 for both the singles and non-fissioning coincidence events, an experimental value of the fission probability was determined. In fig. 16 this ratio is plotted vs the Z of the light fragment. As protons are transferred to the target ($A_3 < 35$), the probability of the heavy fragment undergoing secondary fission increases dramatically. In fact when 5 or more charge units are transferred to Au, essentially all of the heavy fragments ($Z_4 \geq 84$) undergoes secondary fission. For heavy fragments lighter than Au ($Z_3 > 36$), the fissionability falls off very slowly and has a value of 0.2 even after the transfer of 10 charge units. The non zero values of the fissionability for large Z_3 (> 40) is caused by contamination of the singles data by secondary fission events which will have a mean Z of $\sim \frac{1}{2} Z_{tgt}$.

The out-of-plane angular distribution of fission fragments depends both on the Z and E of the light partner in the deep inelastic procers. The FWHM are of the order of 20°-30° in the center of mass of the fissioning nucleus (fig. 17). The interpretation of this width is ambiguous. One possibility is that such width is due to the well-known statistical fluctuation of the fission axis about the normal to the angular momentum. In this case $\sigma_\phi = \sin^{-1} \frac{Ko}{I}$, where $Ko^2 = \frac{\mathcal{J}_{eff}}{\hbar^2} T$ is the standard deviation of the angular momentum projections on the fission axis, $\mathcal{J}_{eff}$ if the effective moment of inertia, and $\bar{I}$ is the average angular momentum of the fissioning nuclei. Since the fission probability biases the angular momentum distribution in favor of high angular momenta, it just may be that $Ko/\bar{I}$ is rather small and that the origin of the out-of-plane angular distributions lies in the second possibility first suggested by Perrin and Péter.[16] This possibility arises from the observation that in the spontaneous fission of ^{252}Cf the fragments have 7-8 $\hbar$ of angular momentum each, oriented perpendicular to the fission axis. A similar effect should arise in deep inelastic processes as well, and to some extent should perturb the alignment of the fragment angular momentum. From statistical arguments the deep inelastic fragment angular momentum distribution arising from this effect should be:

$$P(I) \propto \exp - 2\, I^2/2\mathcal{J}T \qquad (24)$$

where $\mathcal{J}$ is the fragment moment of inertia and T is the temperature. From this we have $\bar{I}^2 = \frac{1}{2}\mathcal{J}T$ or, for our specific case $\bar{I} = 9\hbar$ per

fragment. By coupling this angular momentum in quadrature with the angular momentum arising from the approximately rigid rotation of the complex I_{Rig} we obtain

$$\sigma_\phi = \tan^{-1} \frac{\Gamma}{I_{rig}} \simeq 15° - 18° \qquad (25)$$

This is expected to be so whether the fragment is fissioning or decaying by particle and γ-ray emission. In other words the effect arises from the mechanism of deep inelastic scattering. This effect by itself seems to account for the overall out-of-plane distribution of the fission fragments. One is then led to the tentative conclusion that, because of the fission angular momentum selection, $\frac{K_o}{I_{rig}}$ is small, and that the out-of-plane distribution arises from the very deep inelastic process as a fragment depolarization, rather than from the fluctuations of the angular momentum proejction on the sequential fission axis.

We shall see that γ-ray angular distributions associated with deep inelastic scattering strongly support such a view.

V. γ-RAY EMISSION FROM DEEP INELASTIC EVENTS

The evidence accumulated from high angular momentum compound nuclei shows that the γ-ray multiplicy is an ideal tool for determining the nuclear spin. Since most of the emitted γ-rays arise from stretched E2 decay, the approximate spin of a system is about twice the γ-ray multiplicy. It follows that this method should also be most powerful for the study of the equilibration of rotational degrees of freedom in deep inelastic scattering, because the amount of angular momentum transferred from orbital to intrinsic motion can be directly measured.

Early experiments[9] on 160 Mev ^{20}Ne + ^{Nat}Ag showed that the most relaxed component of the cross-section seems to be associated with rigid rotation of the intermediate complex. On the other hand, the quasi-elastic component and other portions of cross section with varying degrees of inelasticity show a lesser degree of angular momentum transfer. The results of the γ-ray multiplicities in the reaction ^{197}Au + 620 Mev ^{86}Kr are rather puzzling[10]. Even after correction for the events leading to the fission of the heavy recoil, the γ-ray multiplicities fail to rise at low Z values as expected from rigid rotation. This does not seem to be due to lack of rigid rotation after so much mass-transfer nor to the sequential fission removing the largest angular momentum recoils, because experiments with lighter targets seem to lead to similar results. In our opinion the multiplicity does not rise at low Z's because these very asymmetric configuration are populated widely by low ℓ-waves. One can understand this by remembering that for systems of such an entrance channel asymmetry as the present one, the driving force is always in

the direction of symmetry, but it increases dramatically with increasing ℓ-wave. In this way, only the lowest ℓ waves can effectively populate configurations with asymmetries larger than the entrance channel asymmetry. If this is the correct explanation, the measurement of the γ-ray multiplicity becomes a very penetrating tool for the study of the variations in diffusion rate along the mass asymmetry associated with changes in the ℓ-wave. A comparison between some estimates obtained from the diffusion model and the experimental data is shown in fig. 18. The calculation assumes rigid rotation throughout, which is certainly not the case in the vicinity of the projectile. Therefore we should expect a serious failure in this region. However, a few Z's below the projectile the rigid rotation assumption should be adequate and the results more reliable. It is therefore interesting to see that the calculation, just as the data, predicts a levelling off of the γ-ray multiplicities below the projectile Z, without renouncing to the assumption of rigid rotation. A most puzzling point in this field, which, at first sight, seems to destroy the validity of the whole interpretation, is the isotropy of the γ-ray emission within 10%. For stretched E2 radiation emitted by an aligned system one would expect the following angular distribution:

$$W(\theta) = \frac{5}{4}(1 - \cos^4\theta) \quad (E2) \qquad (26)$$

where θ is the angle of the radiation with respect to the normal to the reaction plane. On the other hand the stretched E1 radiation has an angular distribution given by:

$$W(\theta) = \frac{3}{4}(1 + \cos^2\theta) \quad \text{(E1)} \qquad (27)$$

Even under the very unlikely assumption of 50% E2, 50% E1 stretched radiations, one should observe an anisotropy $W(90°)/W(o^c) = 1.33$. The apparently devastating conclusion of non-stretched γ-ray emission can be avoided if we assume that the angular momentum of the fragements from deep inelastic processes is not aligned. But this is exactly the second possibility invoked in interpreting the sequential fission out-of-plane angular distribution. A misalignment of $\pm$ 15°-20° generated in the bending oscillations of the intermediate complex, together with 10-20% E1 radiation easily explains the γ-ray isotropic distribution. In this way it is apparent that the γ-ray multiplicity technique is in some way complementary to the sequential fission method in assessing the dynamical situation for the rotational degrees of freedom.

CONCLUSION

From this brief and sketchy presentation it is possible to glimpse the great wealth of physically interesting features associated with heavy ion reactions. The fortunate range of lifetimes of the intermediate complex offers the possibility of measuring relaxation times associated with a variety of degrees of freedom. This experimental availability gives the dynamical and non-equilibrium statistical many-body aspects of t nuclear matter the rightfully prominent pl ce they clearly deserve.

REFERENCES

1. L.G. Moretto and R. Schmitt, Journal de Physique, C5, No. 11, 37(1976) 109 and references therein.
2. J. Galin, Journal de Physique C5, No.11, 37(1976) 83 and references therein.
3. L. G. Moretto and J. S. Sventek: Phys. Lett. B58 (1975) 26
4. W. Nörenberg, Z Physik A274 (1975) 241.
5. L. G. Moretto, Proceeding on the International Conference on Reaction Models Balatonfüred, Hungary 1977 - Preprint NBI-77-16
6. B. Cauvin, R. Jared, P. Russo, R. Babinet, R. Schmitt and G. Moretto, to be published.
7. R. P. Schmitt, G. Bizard, G.J. Wozniak and L. G. Moretto, to be published.
8. G. J. Wozniak, P. Glässel, RP. P. Schmitt, J. M. Moulton, G. Bizard R. C. Jared and L. G. Moretto, to be published.
9. P. Glässel, R. S. Simon, R. M. Diamond, R. G. Jared, I. Y. Lee, L. G. Moretto, J. O. Newton, R. Schmitt and F. Stephens, Phys. Rev. Lett. 38 (1977) 331
10. Preliminary results from the Moretto and Diamond-Stephens groups, Berkeley.
11. J. Randrup, Procedding of the International Workshop on Gross Properties of Nuclei and Nuclear Excitations, AED- Conf. 77-017-001, Hirschegg,1977.
12. J. Block, J. Randrup, W. J. Swiatecki and C. F. Tsang, LBL 5014 (1976).

13. P. Russo, R. P. Schmitt, G. J. Wozniak, R. C. Jared, P. Glässel, B. Cauvin, J. S. Sventek and L. G. Moretto, Nucl. Phys A281 (1977) 509.

14. B. Cauvin, R. P. Schmitt, G. J. Wozniak, P. Glässel, P. Russo, R. G. Jared, J. B. Moulton and L. G. Moretto, LBL 6506 (1977).

15. P. Russo, R. P. Schmitt, G. J. Wozniak, B. Cauvin, P. Glassel, R. G. Jared and L. G. Moretto, Phys. Lett. 67B (1977) 155.

16. N. Perrin and J. Peter, IPNO-RL-77-02.

Work performed under the auspices of the U. S. Energy Research and Development Administration.

FIGURE CAPTIONS

Fig. 1 Top. Dependence of the interaction time upon angular momentum at three bombarding energies for the reaction Au + Kr.
Bottom. Average deflection functions for the same bombarding energies.

Fig. 2 Angle integrated Z distributions for the reaction Au + 600 MeV Kr (a) and for Ta + 620 MeV Kr (b). The dots are the experimental points and the solid line the theoretical calculation.

Fig. 3 Angular distributions of fragments of selected Z for the reaction Au + 600 MeV Kr (a) and for Ta + 600 MeV Kr (b). The dots are the experimental points and the solid lines the theoretical calculations.

Fig. 4 Comparison of experimental and calculated energies of the scattered projectile and target in the elastic scattering of 163 MeV ^{40}Ar on Au(x), Ag(0), and Cu(●).

Fig. 5 Total number of nucleons evaporated by the fragments.

Fig. 6 a) Masses before evaporation and number of evaporated nucleons close to symmetric splitting as a function of the fragment Z after evaporation.
b) Same quantities as in a) as a function of the fragment Z before evaporation.

Fig. 7 Masses before evaporation and mean number of neutrons as a function of the fragment Z before evaporation. The upper solid line is calculated assuming mass to charge equilibrium between two touching spheres of fixed mass ratio. The dashed line is obtained from an evaporation calculation.

Fig. 8 Top. Standard deviations of the out-of-plane (Lab.system) angular distributions of the heavy fragments. The dashed line has been calculated assuming that all the evaporated particles are neutrons, while the solid line has been calculated assuming the evaporation of the proper amount of neutrons, protons and α particles. Bottom. Same as above for the in-plane angular distributions. The dashed line is calculated assuming the evaporation of neutrons, protons and α particles. The kinematical broadening due to the fluctuations in kinetic energy has been included.

Fig. 9 Distributions of Z2 for Z = 16 for various bins in total kinetic energy.

Fig. 10 Missing charge as a function of total kinetic energy for various values of Z1 and at various values of θ2.

Fig. 11 Average missing charge as a function of total kinetic energy for three values of the out-of-plane angle.

Fig. 12 Average missing charge as a function of total kinetic energy for three beam energies.

Fig. 13 Calculated average charge of an evaporated particle as a function of temperature. Δ is the difference between the α and proton effective barrier, while δ is the difference between the neutron and proton effective barrier.

Fig. 14 Relative amounts of fissioning and non-fissioning heavy fragment as a function of the kinetic energy of the light fragment. The upper scale represents an estimate of the heavy fragment excitation energy.

Fig. 15 Fraction of the heavy fragments undergoing fission as a function of the light fragment kinetic energy. The upper scale represents an estimate of the heavy fragment excitation energy.

Fig. 16 Average fission probabilities of the heavy fragment as a function of the Z of the light fragment.

Fig. 17 Lab and center of mass FWHM of the out-of-plane angular distributions of fission fragments as a function of the Z of the light fragment.

Fig. 18 Experimental and theoretical γ-ray multiplicities as a function of Z. The large band represent the theoretical width (± σ) which is also plotted in the lower part of the figure.

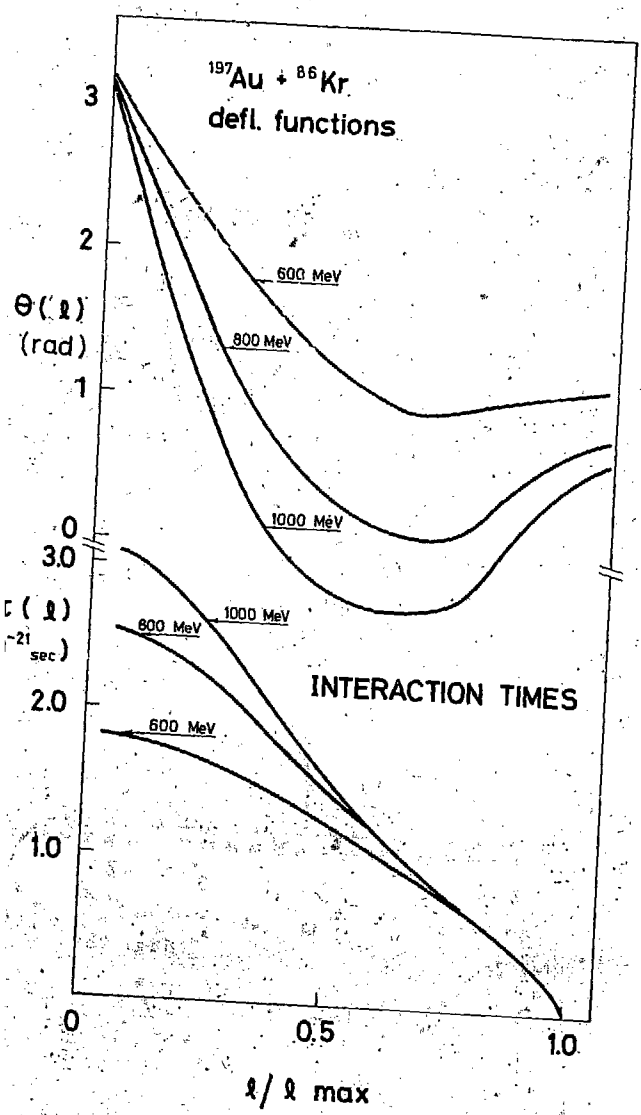

XBL 778-9815

Fig. 1

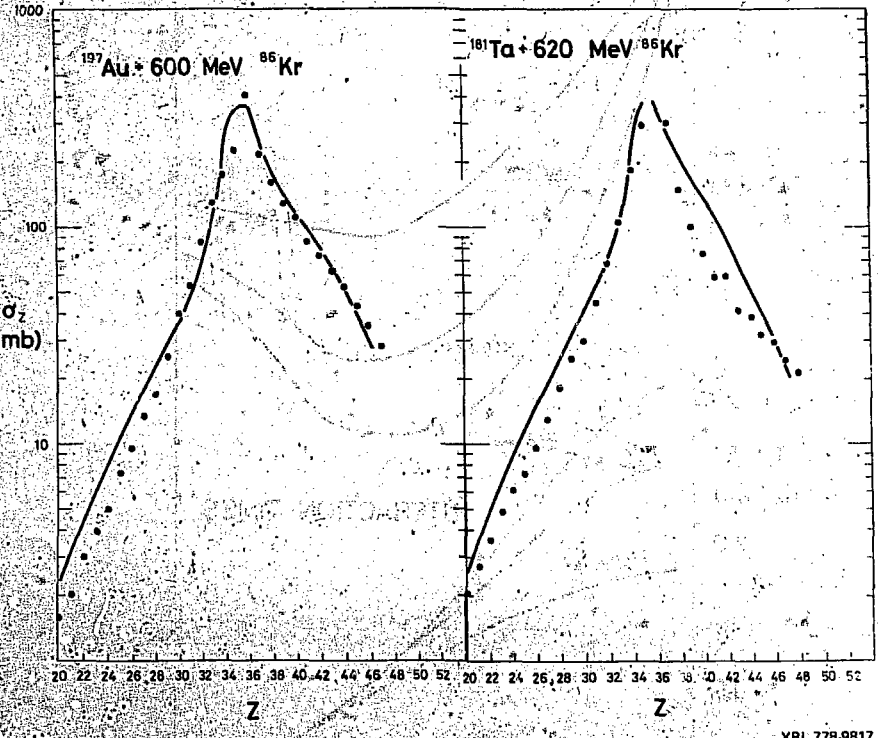
197Au + 600 MeV 86Kr
181Ta + 620 MeV 86Kr
1000
100
10
σz (mb)
20 22 24 26 28 30 32 34 36 38 40 42 44 46 48 50 52
Z
XBL 778-9817

Fig. 2a

Fig. 2b

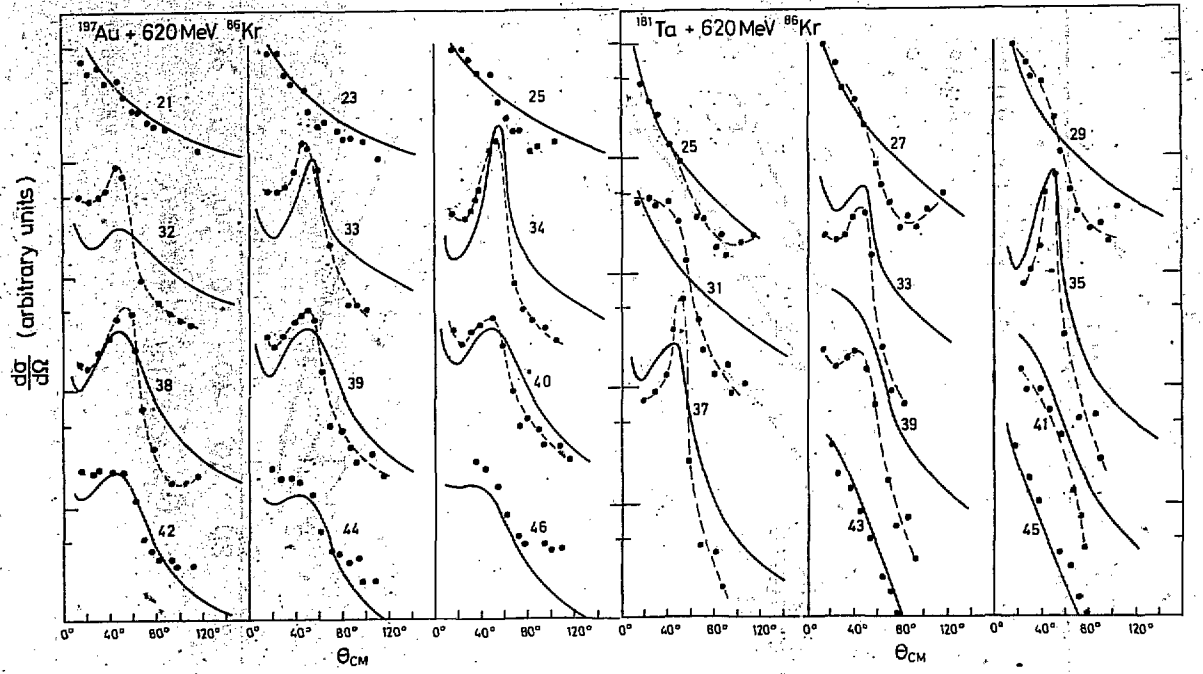

XBL 778-9908

Fig. 3a

Fig. 3b

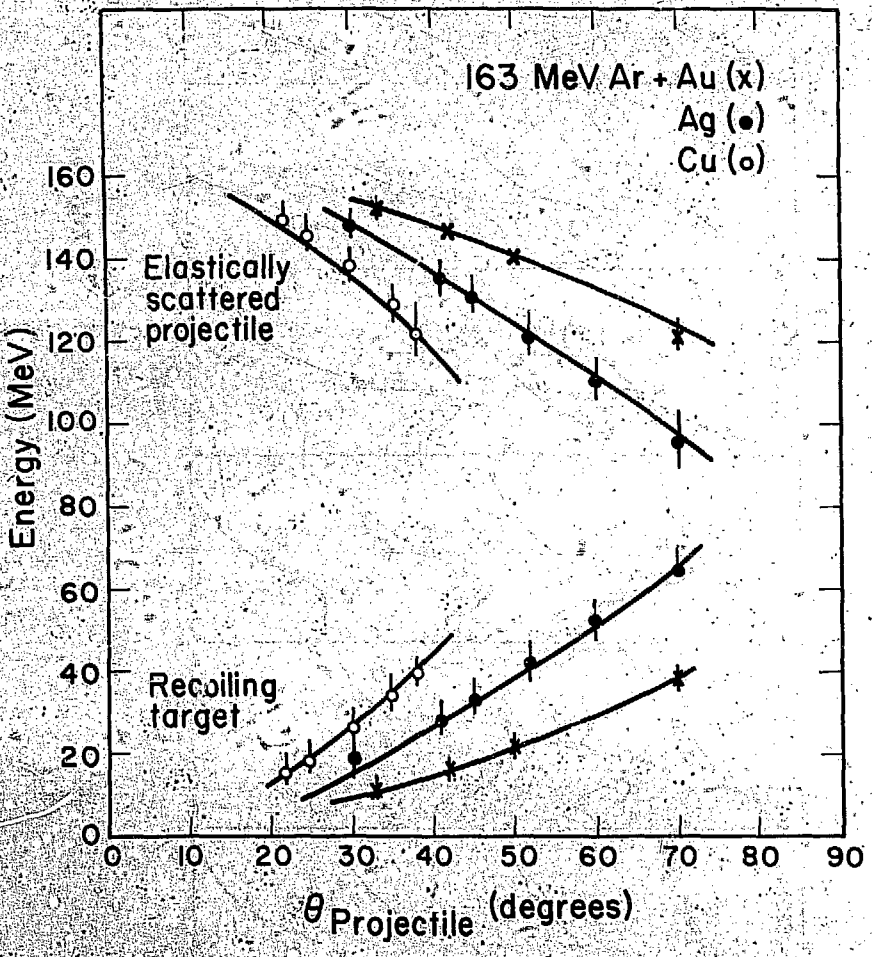

XBL 766-8213

Fig. 4

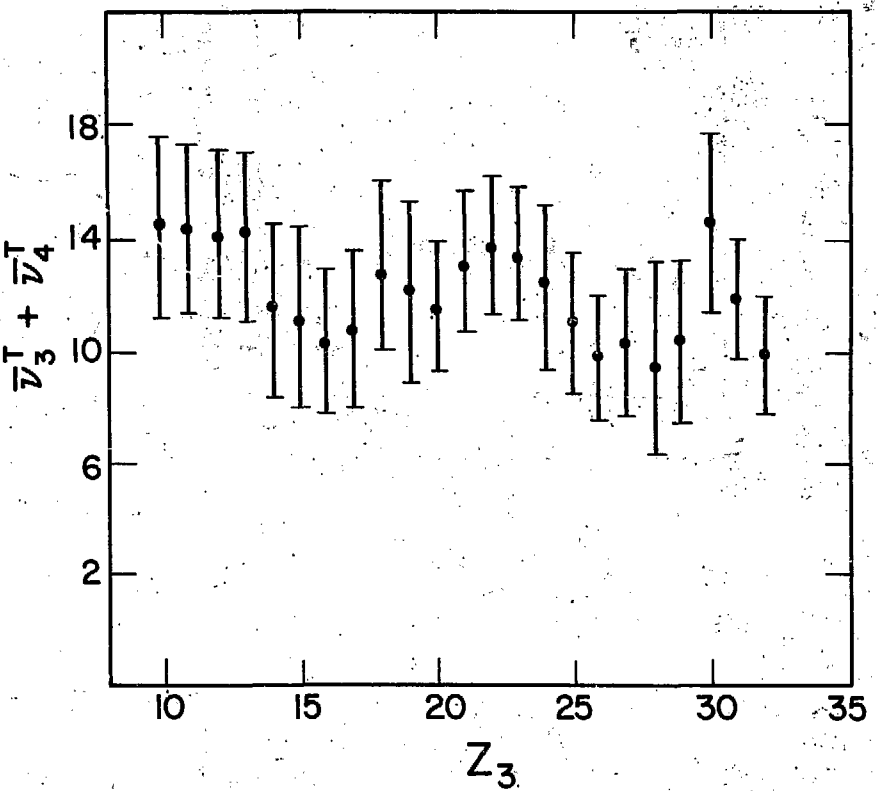

XBL 778-1731

Fig. 5

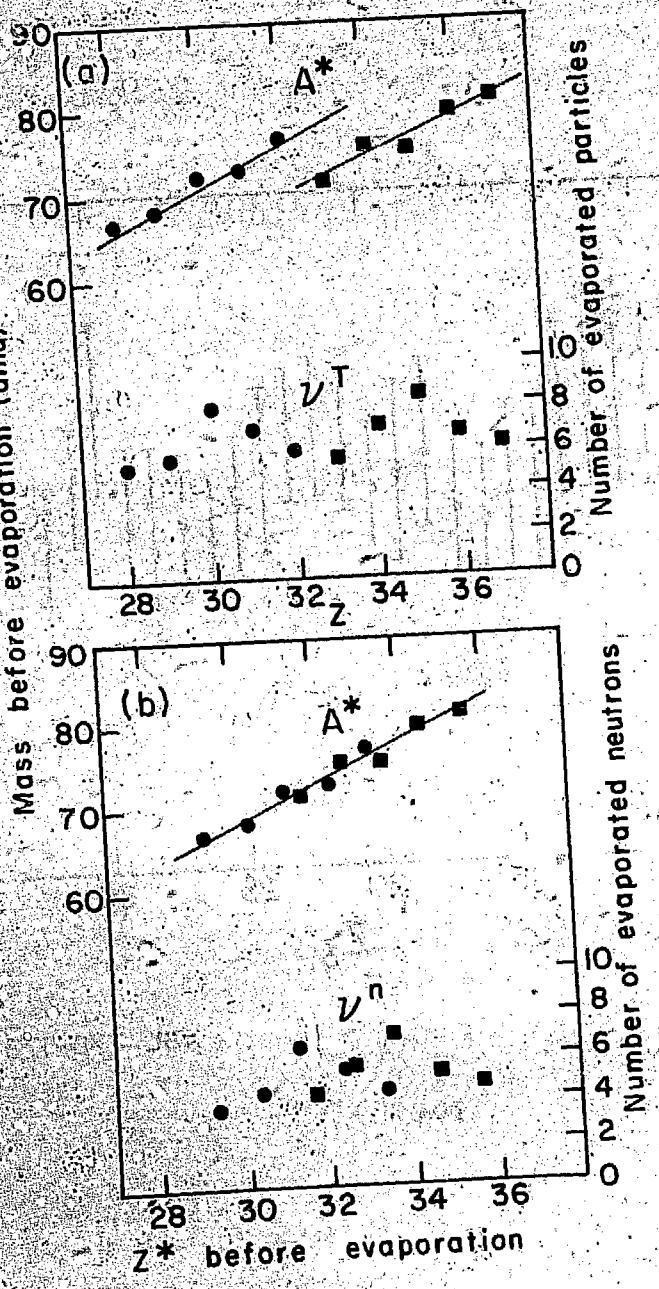

XBL766-8209

Fig. 6

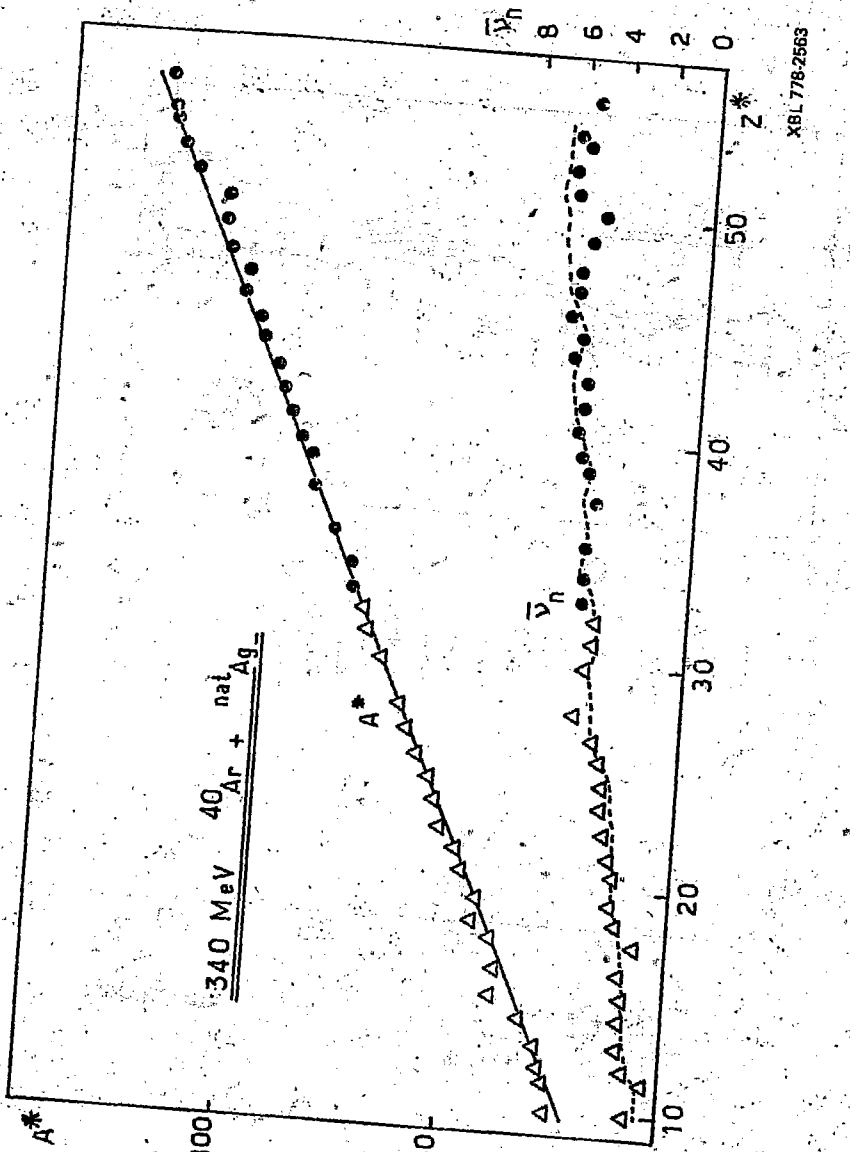
A*
100
50
0
10
20
30
40
50
Z*
8
6
4
2
0
$\bar{\nu}_n$
340 MeV ^{40}Ar + ^{nat}Ag
A*
$\bar{\nu}_n$
XBL 778-2563

Fig. 7

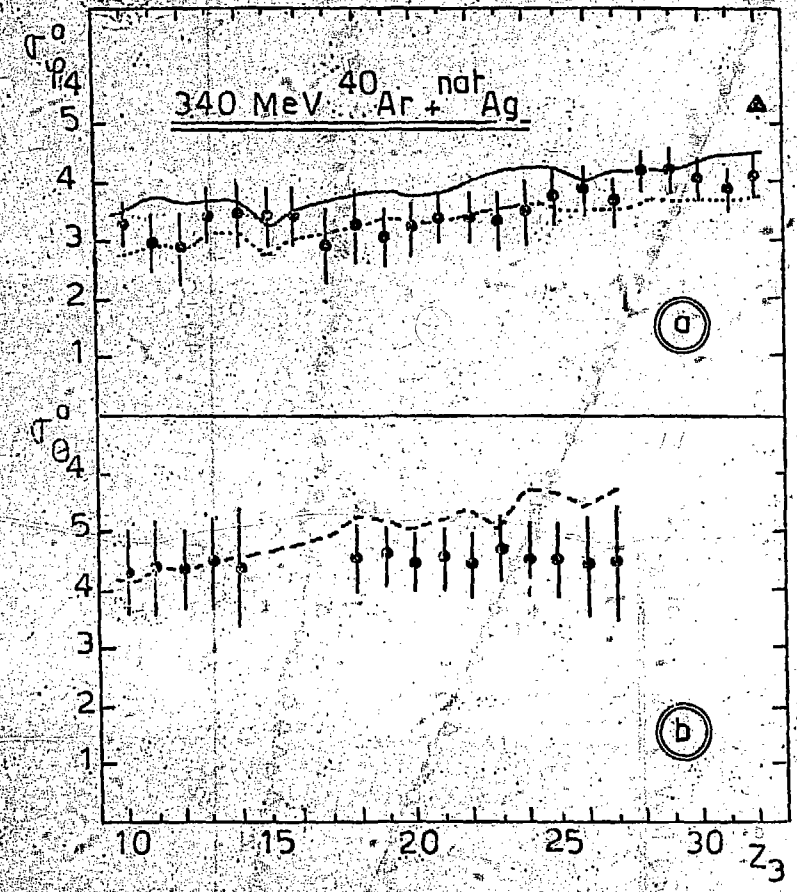

XBL 778-2624

Fig. 8

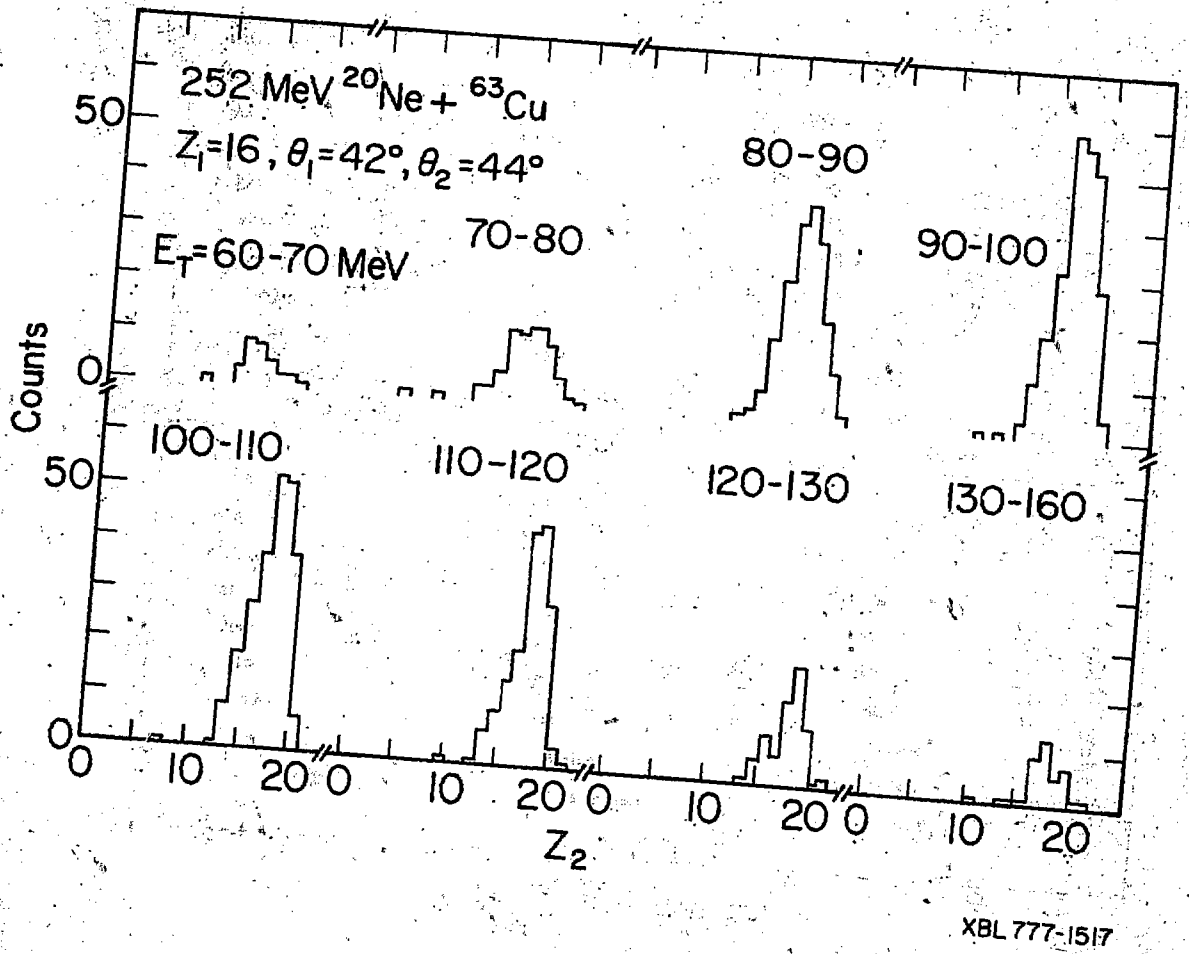
252 MeV ^{20}Ne + ^{63}Cu
Z_1=16, θ_1=42°, θ_2=44°
E_T=60-70 MeV
70-80
80-90
90-100
100-110
110-120
120-130
130-160
Counts
50
0
50
0
0
10
20
0
10
20
0
10
20
0
10
20
Z_2
XBL 777-1517

FIG. 9

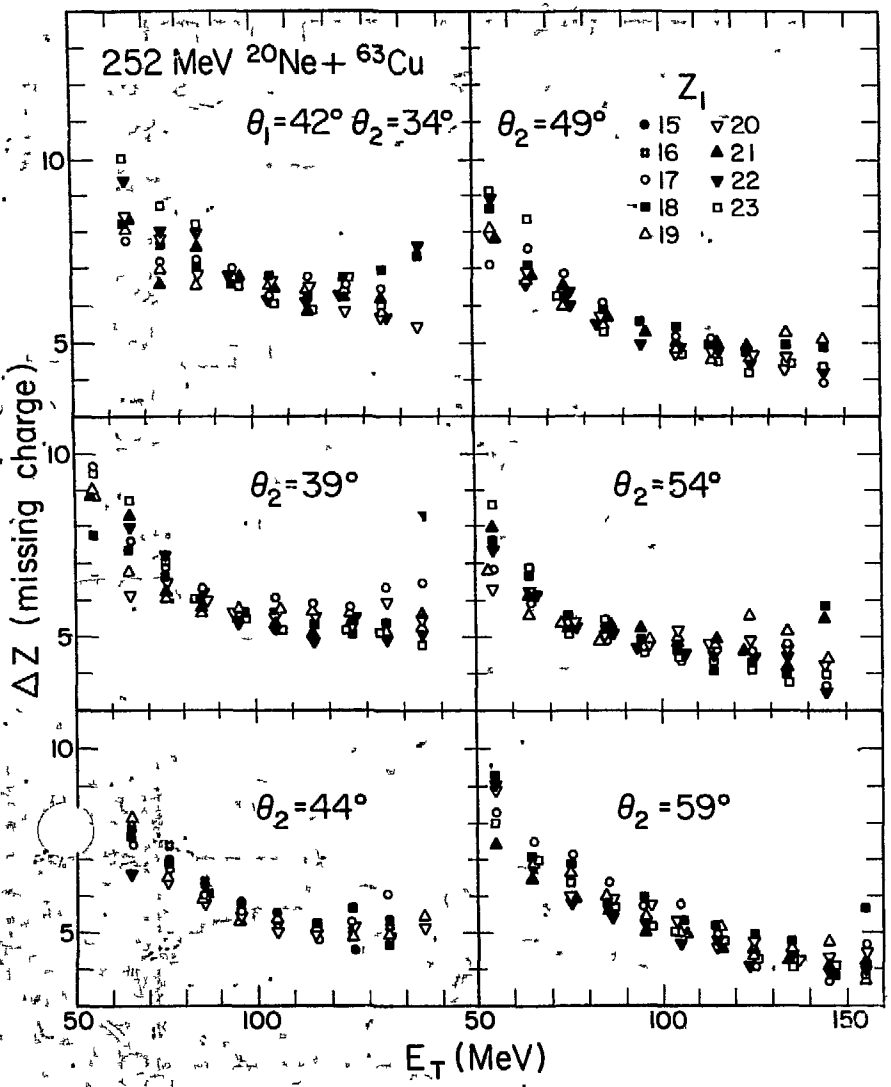

XBL777-1408

Fig. 10

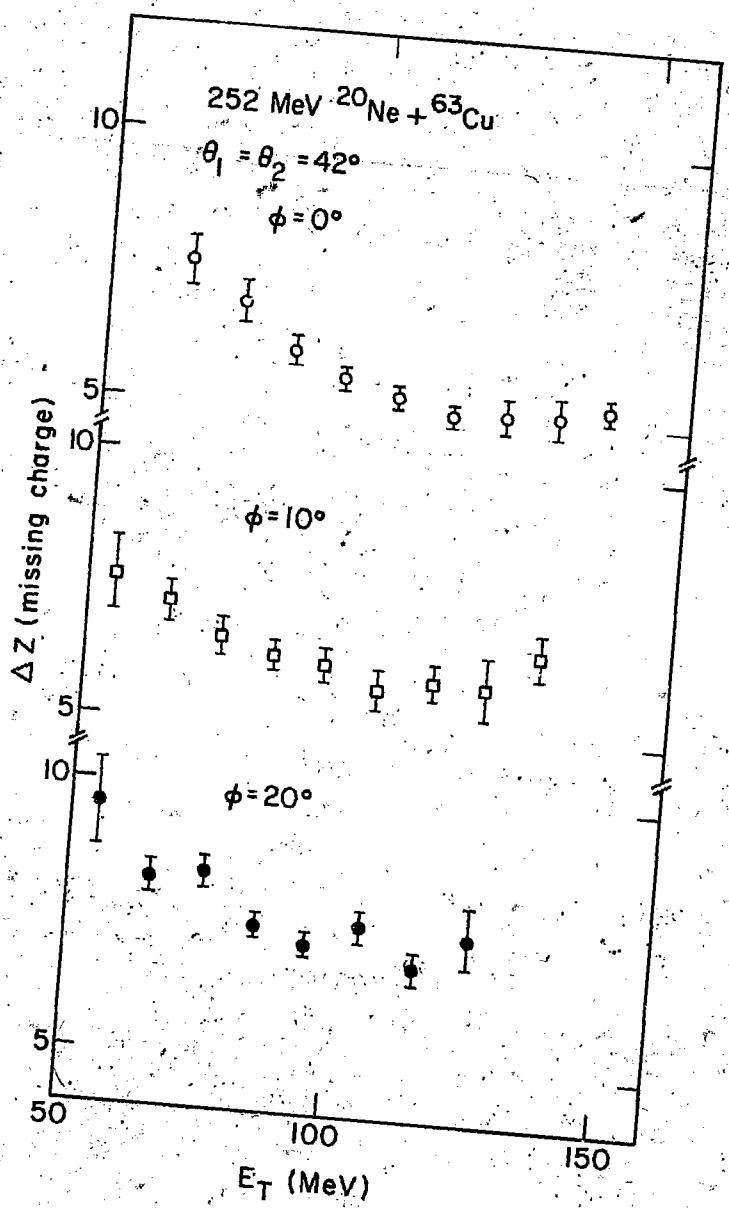

Fig. 11

XBL777-1398

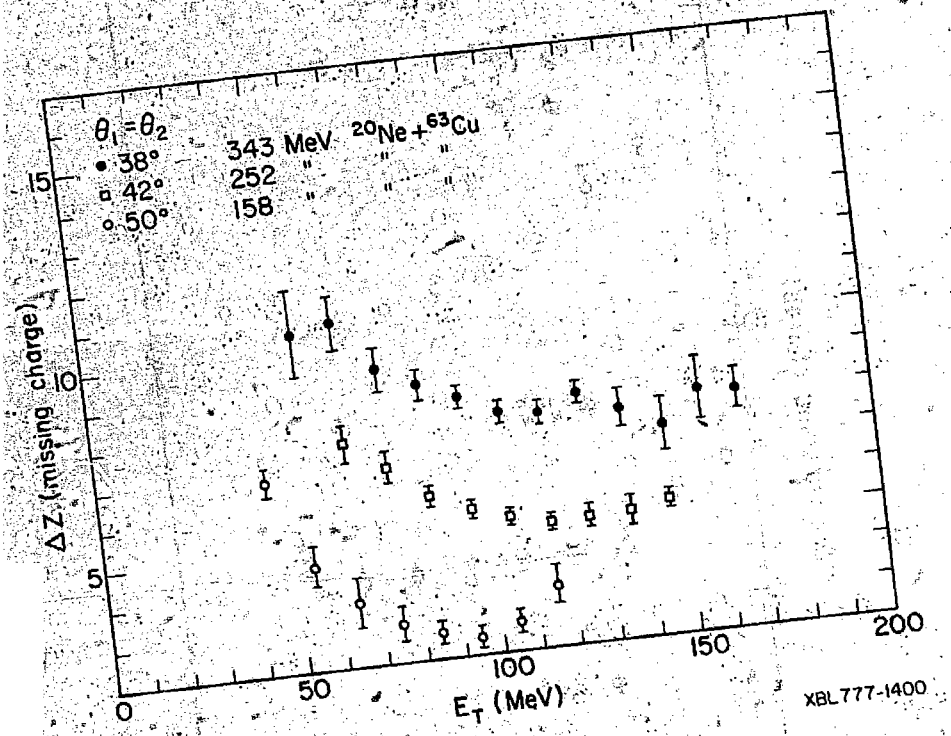
$\theta_1 = \theta_2$
• 38°
□ 42°
○ 50°
343 MeV $^{20}Ne + ^{63}Cu$
252 " " "
158 " " "
ΔZ (missing charge)
E_T (MeV)
0
50
100
150
200
5
10
15
XBL777-1400

Fig. 12

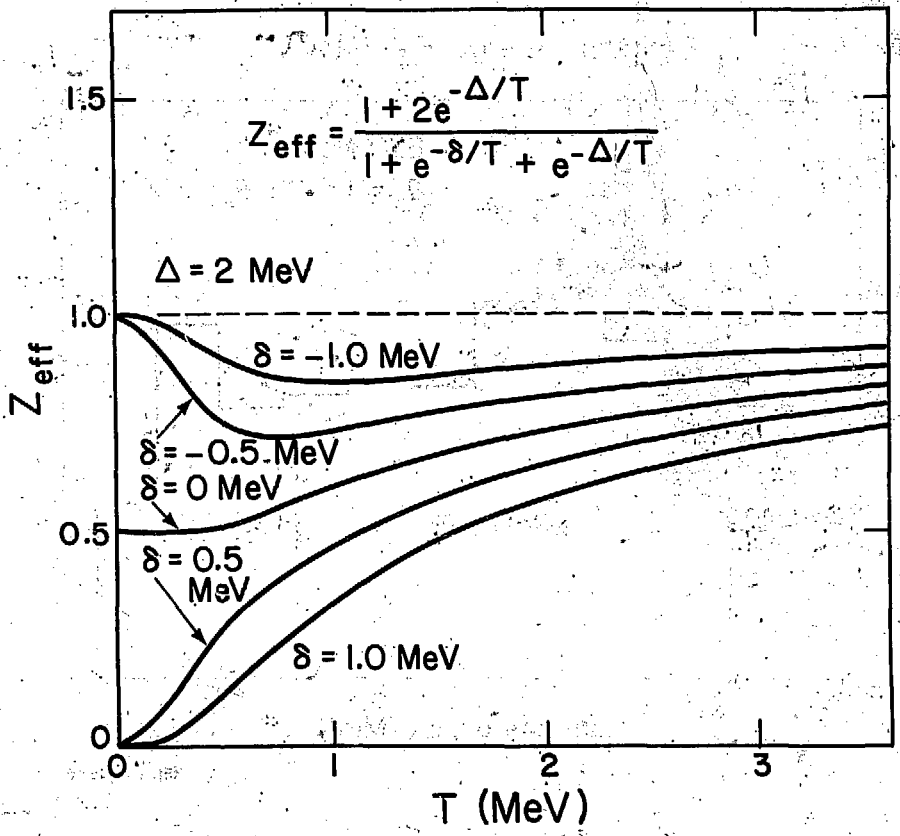

XBL 778-1662

Fig. 13

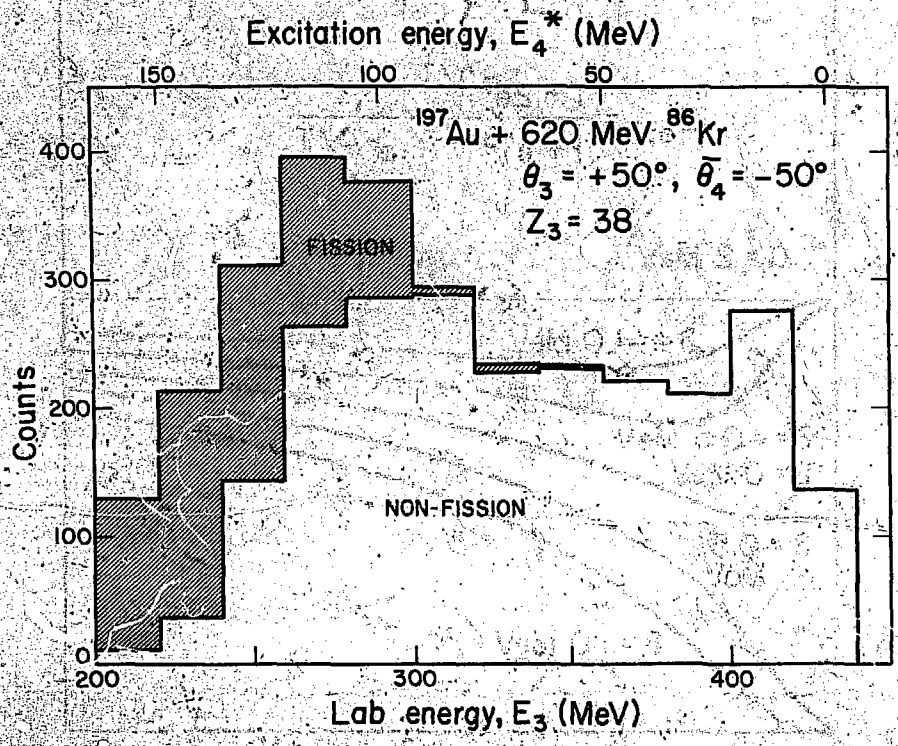
Excitation energy, E_4^* (MeV)
150
100
50
0
^{197}Au + 620 MeV ^{86}Kr
$\theta_3 = +50°$, $\theta_4 = -50°$
$Z_3 = 38$
FISSION
NON-FISSION
Counts
400
300
200
100
0
200
300
400
Lab energy, E_3 (MeV)
XBL 778-1666

Fig. 14

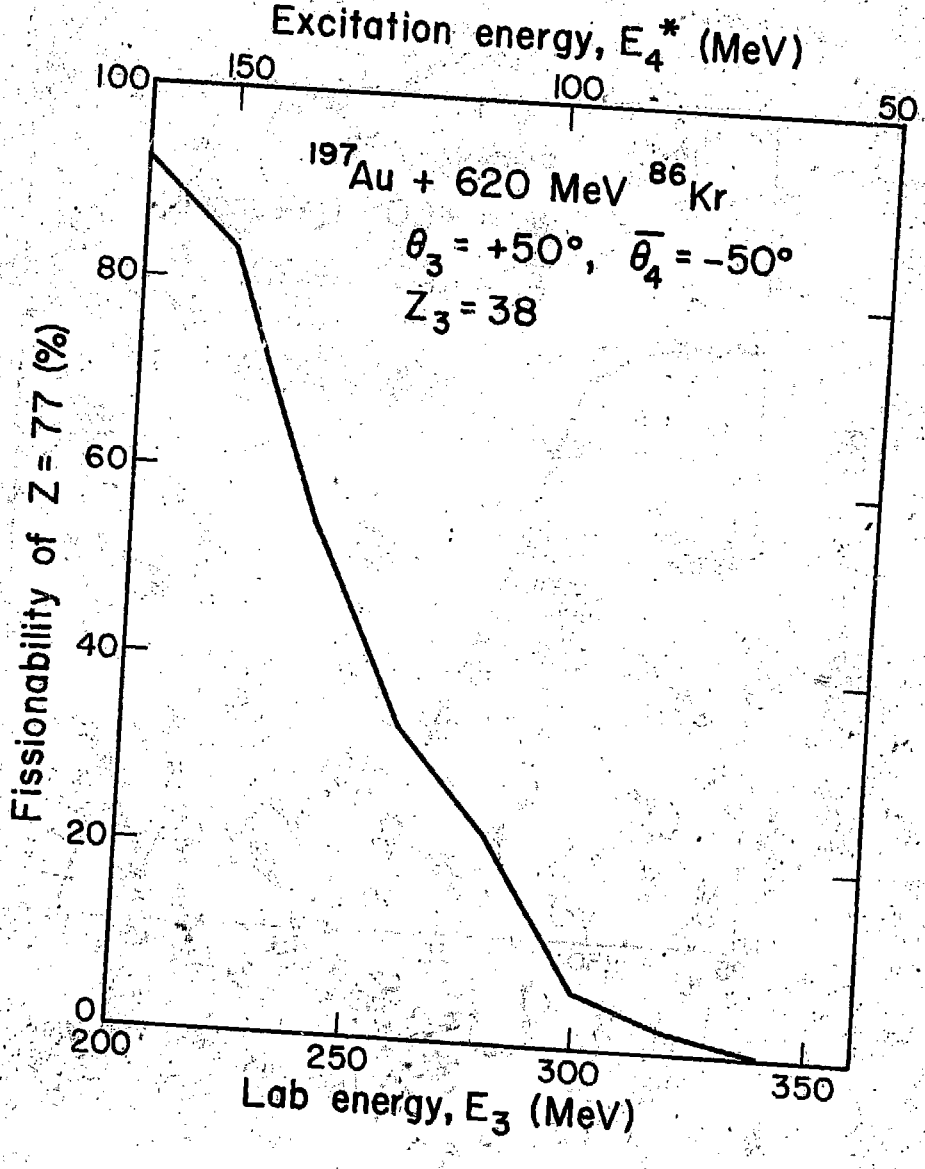

Fig. 15

XBL 778-1665

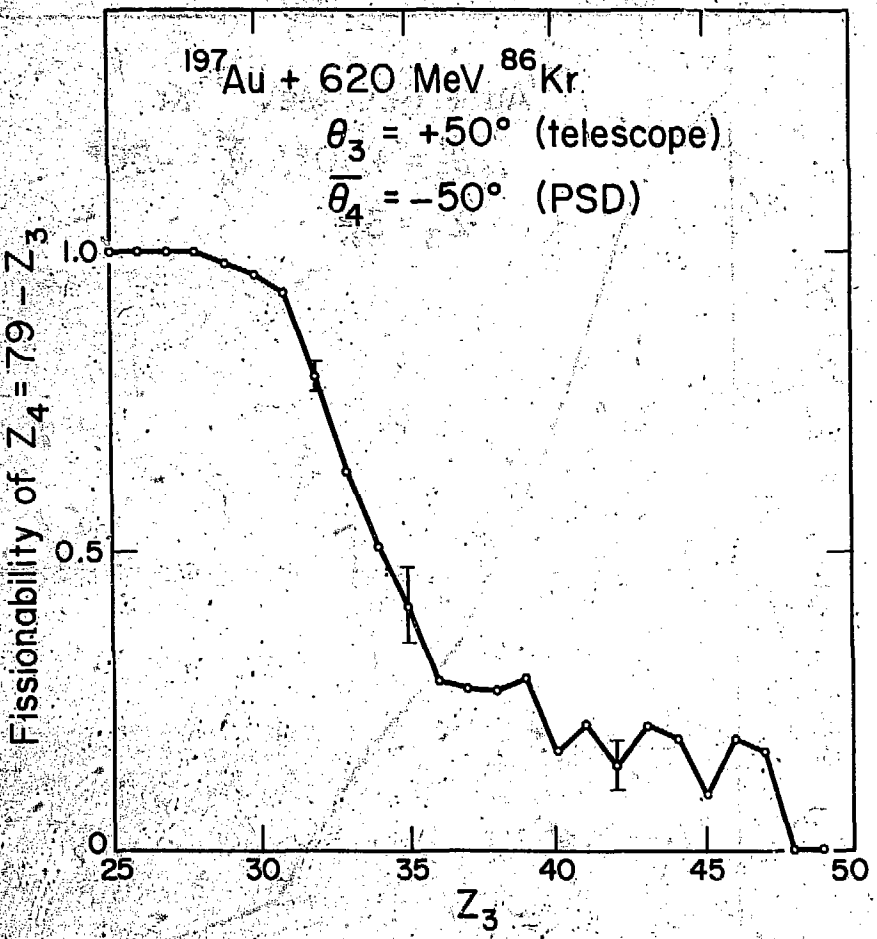

XBL 778-1664

Fig. 16

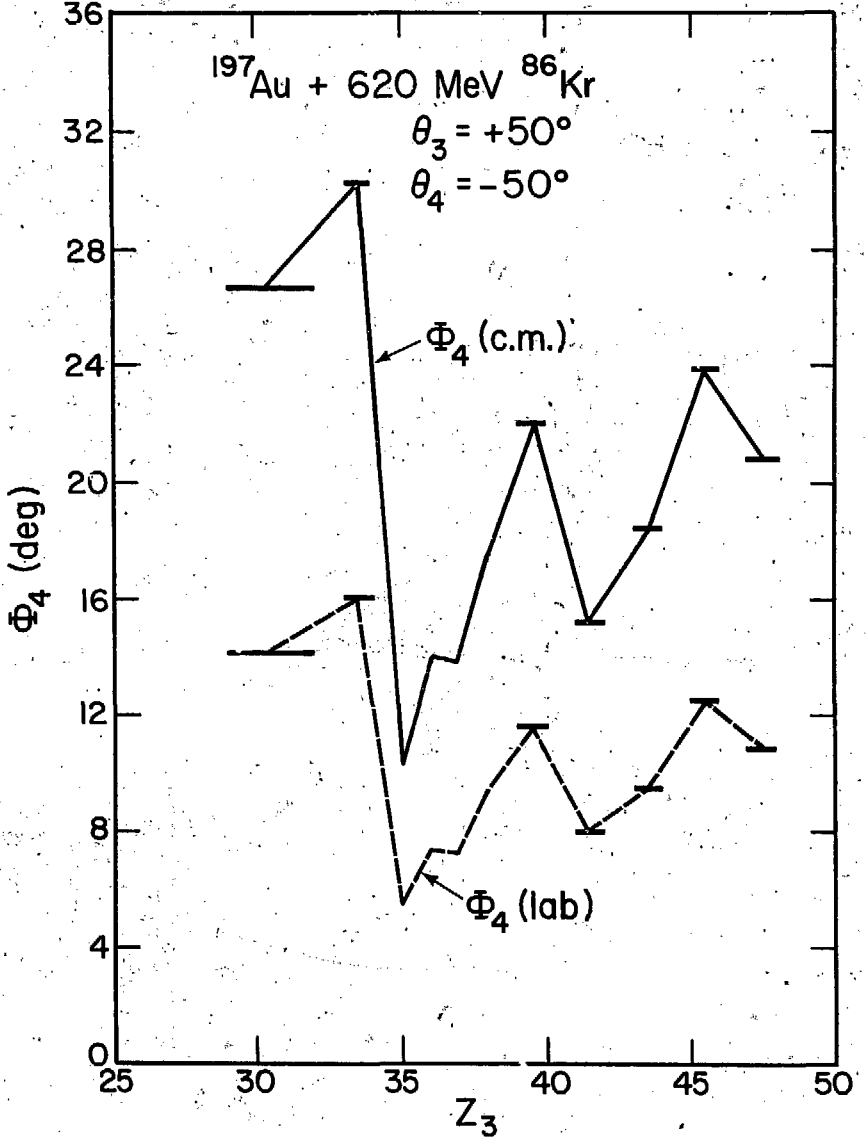

XBL 778-1663

Fig. 17

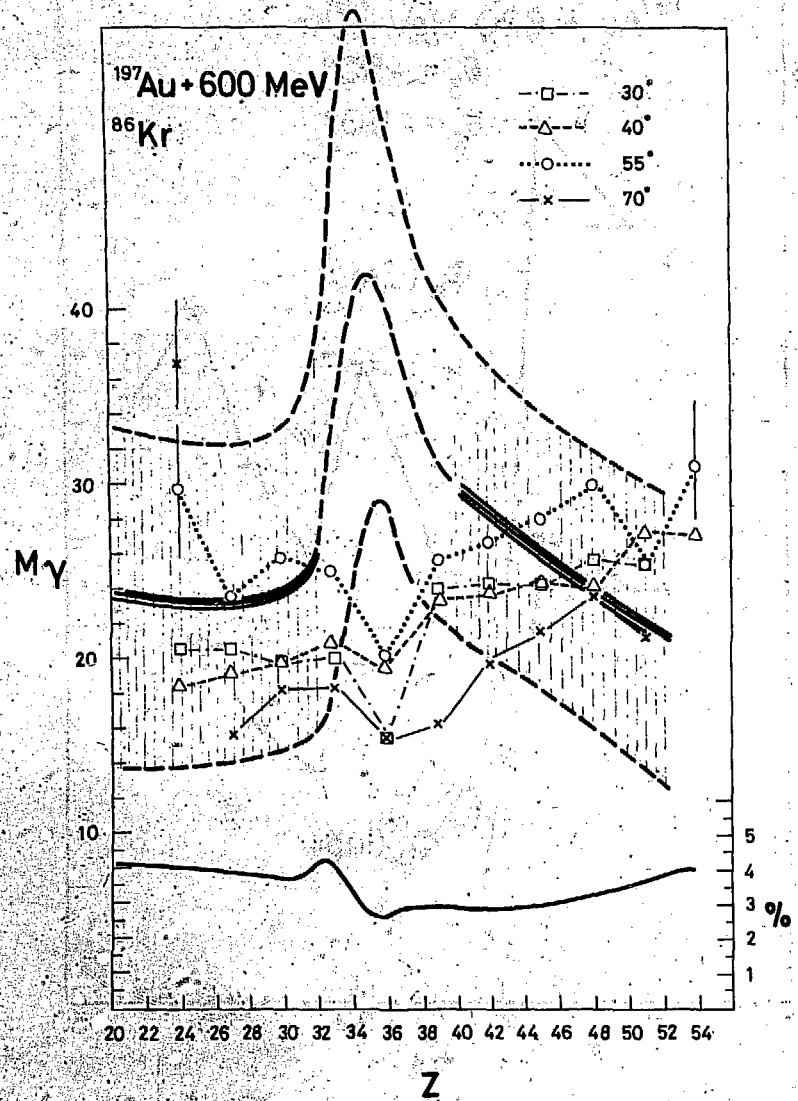

XBL 778-9813

Fig. 18